Polymer Composites

WILEY | spe INSPIRING PLASTICS PROFESSIONALS

RESEARCH ARTICLE OPEN ACCESS

Accelerated Degradation of PLA-Based Composites in Harsh Alkaline Environment

Cristina Moliner[1] | Alberto Lagazzo[1] | Juan Felipe Basbus[1,2] | Roberto Raiteri[3] | Elisabetta Finocchio[1] | Elisabetta Arato[1,4]

[1]Department of Civil, Chemical and Environmental Engineering (DICCA), University of Genova (UniGe), Genoa, Italy | [2]Aragón Nanoscience and Materials Institute (INMA), Higher Council for Scientific Research (CSIC), University of Zaragoza (UniZar) and Condensed Matter Physics Department, Zaragoza, Spain | [3]Department of Informatics, Bioengineering, Robotics and Systems Engineering (DIBRIS), Genoa, Italy | [4]TICASS s.c.r.l., Genoa, Italy

Correspondence: Elisabetta Finocchio (elisabetta.finocchio@unige.it)

Received: 19 November 2025 | **Revised:** 10 March 2026 | **Accepted:** 16 March 2026

Keywords: calcium silicate | degradation mechanisms | glass fiber | harsh conditions | polylactic acid

ABSTRACT

The performance of poly(lactic acid) (PLA) bioplastics under harsh service conditions must be understood to enable their use in multi-use products. This work aims to investigate the accelerated degradation of PLA-based composites designed for multi-use cutlery and rigid packaging when exposed to an alkaline environment (pH 12, 70°C) for 30 days. Two formulations were studied: PLA reinforced with glass fibers (C) and with calcium silicate (RP). Mechanical testing, Scanning Electron Microscopy (SEM), Atomic Force Microscopy (AFM), Fourier Transform Infrared Spectroscopy in Attenuated Total Reflectance (FTIR-ATR), and X-ray diffraction were used to correlate changes in tensile properties, surface morphology, chemical structure, and crystallinity. After aging, both composites showed strong embrittlement, with ultimate tensile strength dropping from about 80 to 25 MPa for the cutlery grade and from about 54 to 24 MPa for the rigid packaging grade, and strain at break decreasing from around 2% to below 1%. Surface analysis revealed pronounced erosion, microcrack formation, and a significant increase in roughness, especially for the calcium-silicate-filled composite, while FTIR-ATR and XRD indicated ester bond hydrolysis and higher overall crystallinity. These results demonstrate that the type of reinforcement critically controls degradation mechanisms and residual properties, providing guidelines for the design of more durable PLA-based bioplastics for demanding dishwasher-like and other harsh alkaline applications.

1 | Introduction

Rising environmental concerns regarding plastic pollution have driven the adoption of sustainable bioplastics as alternatives to conventional plastics in multi-use cutlery and rigid packaging [1] in food-contact applications, where materials must withstand repeated exposure to elevated temperatures, alkaline detergents, and mechanical stress during industrial dishwashing cycles while maintaining structural integrity, food safety, and biodegradability [2, 3].

Poly(lactic acid) (PLA) offers high stiffness and renewability but suffers from brittleness and poor thermal stability above its glass transition temperature ($T_g \approx 60°C–65°C$), which limits its durability in demanding, repeated-use applications [4]. To overcome these limitations, several strategies have been explored. These include polymer blending (e.g., with poly-D-lactide) to enhance crystallinity and heat resistance [5], incorporation of nanofillers (e.g., cellulose nanocrystals) to improve elongation and toughness [6], and chemical modifications to enhance thermal, mechanical, and barrier properties [7]. Moreover, the presence of inorganic fillers such as silicates has been reported to improve the crystallinity of the composites and then correlated to an improvement of their mechanical properties [8, 9]. At the research level, PLA-based engineered blends and biocomposites are being extensively studied [10]. At the commercial scale, NatureWorks LLC and Corbion are the two major producers of PLA [11], and crystallized PLA (CPLA) formulations containing mineral fillers such as chalk or talc are used to produce heat-resistant cutlery capable of handling foods at high temperatures [12].

Highlights

- PLA-based polymer was reinforced with glass fibers or calcium silicate and exposed under harsh alkaline conditions.
- Biocomposites post-treatment evidenced an embrittlement with respect to pristine samples.
- Post-treatment samples indicated surface degradation, chemical, and crystallinity modifications.
- Polymeric chains would suffer a reorganization in a harsh alkaline environment.
- Reinforcement type plays a critical role in the performance under harsh alkaline conditions.

The durability of such PLA biocomposites critically depends on the interplay between environmental exposure, crystallinity and reinforcement type. Hydrolytic degradation of PLA is accelerated by temperature, pH, and molecular structure, as demonstrated by our previous research [13]. At or above the glass transition temperature ($T_g \approx 60°C–65°C$), PLA chains become more flexible, enhancing hydrolysis rates due to increased water diffusion into amorphous regions, where degradation preferentially initiates [14]. Environmental pH also critically affects degradation: basic conditions (pH > 7) catalyze ester bond cleavage via hydroxide ions (OH^-), depolymerizing PLA into lactide oligomers [15, 16], while acidic media (pH < 4) promote autocatalytic degradation through carboxylic acid end groups ([17, 18]).

Crystallinity modulates degradation rates, with amorphous regions degrading more rapidly than crystalline domains [19]. The presence and nature of reinforcing agents can also significantly impact the crystallinity of biocomposites by, for example, providing additional nucleation sites during the crystallization process [20]. It is widely reported that fibers such as glass or silicates increase the crystallinity of bioplastics when incorporated into their formulation [21], thereby enhancing the initially low mechanical strength of the polymer. Moreover, the choice of an appropriate reinforcing agent can be used to tune the balance between amorphous and crystalline phases, modifying material behavior for specific applications [22].

As shown, prior studies have examined neat PLA or model composites under hydrothermal/alkaline aging, and others have characterized glass fiber- or silicate-reinforced PLA for mechanical enhancement, but few have investigated commercial formulations designed specifically for multi-use cutlery and food packaging under dishwasher-like conditions (70°C, pH 12). Prior work rarely combines tensile testing, micro/nanoscale morphology (SEM/AFM), chemical characterization (FTIR-ATR), and crystallinity evolution (XRD), nor systematically compares how glass fibers and calcium silicate control water uptake, degradation pathways, and residual properties.

This study fills this gap by characterizing two commercial PLA composites, one for cutlery (glass fiber-reinforced) and one for rigid packaging (calcium silicate-reinforced), before and after accelerated aging at 70°C and pH 12 for 30 days. These specific conditions were chosen based on our previous results investigating the effect of pretreatment in several media and temperatures on one of the PLA-based composites [4]. Comprehensive analysis reveals reinforcement-specific degradation mechanisms, providing design guidelines for durable, sustainable PLA bioplastics capable of withstanding repeated dishwashing while meeting food-contact and end-of-life requirements.

2 | Materials and Methods

2.1 | Materials and Sample Preparation

PLA-based polymer samples filled with glass fibers (20% in weight) were provided by Arctic Biomaterials OY Ltd., Oulu, Ostrobothnia, Finland. They were designed to produce multi-use cutlery (samples labeled with a C) by means of injection molding. Another PLA-based polymer with calcium silicate as a mineral filler (30%, in weight), ArcBiox MFA30-B2000, and processed through injection molding, provided by Arctic Biomaterials OY Ltd. again was designed for its use as multi-use rigid packaging (RP). Further details on the polymer matrix formulations are confidential due to the reserved nature of the tested specimens.

The accelerated aging tests were performed in laboratory-controlled conditions. The time (t) was fixed at 30 days to obtain sensitive differences between fresh and treated samples [13]. For this work, a $T = 70°C$ and pH = 12 were selected as the highly aggressive conditions, leading to relevant degradation phenomena, based on results reported by us in previous studies on PLA-based C samples [4]. Samples were labeled as C/RP-T-pH (Table 1) to indicate the type of sample (C-cutlery and RP-rigid packaging), the temperature of immersion treatment (70°C) and the pH of the immersion medium (12).

2.2 | Methods

2.2.1 | Mechanical Tests

Tensile tests were performed according to the Standard DIN EN ISO 527-1 on dog-bone specimens at room temperature with an electro-mechanical universal testing machine Zwick/Roell Z50 (ZwickRoell GmbH & Co. KG, Ulm, Baden-Württemberg, Germany), equipped with a modular sensor arm extensometer makroXtens II and a load cell of 50 KN. All the tests were run with a rate of 1 mm/min for the determination of the Tensile Elastic Modulus and with a rate of 50 mm/min until break. The

TABLE 1 | Experimental conditions and nomenclature.

Type	Experimental conditions			Nomenclature
	T (°C)	pH	t (d)	
Rigid packaging (RP)	—	—	0	RP benchmark
	70	12	30	RP-70-12
Cutlery (C)	—	—	0	C benchmark
	70	12	30	C-70-12

mechanical results were: Young's Modulus (E_t), Ultimate Tensile Strength (UTS, σ_M) as the maximum stress recorded during the test, Strain at UTS (ε_M), and Strain at break (ε_B).

2.2.2 | Scanning Electron Microscopy

The morphological analysis was performed with a Scanning Electron Microscope Hitachi S-2500 (Hitachi High-Tech Corporation, Tokyo, Tokyo Metropolis, Japan), in secondary electron mode. A portion of about 5 mm was obtained from the samples used for the tensile tests. The samples were observed, after gold coating, on the external surface at 25×, 100×, 500×, and 1000× magnifications.

2.2.3 | Wetting Test

Static contact angle tests were performed using an experimental device developed at DICCA-UniGe. Distilled water droplets, standardized in size and kept small to minimize gravitational effects, were dispensed from a precision pipette and placed in contact with the solid surface of the samples. A digital Dino Lite microscope was employed to capture images of metastable droplets on the samples' surface after approximately 5 s. The contact angle was evaluated graphically using Autodesk AutoCAD software.

2.2.4 | Atomic Force Microscopy

Atomic force microscopy measurements were obtained using a Nanowizard 4 JPK AFM (Bruker corporation, Berlin, Berlin, Germany) equipped with an additional scanner (HydridStage, Bruker) to extend the vertical range during scanning to follow the topography of the surface. Square $100\times100\,\mu m^2$ areas were randomly selected on the sample surface and scanned in contact mode to obtain 512×512 pixel topography images. Samples were scanned in pure (MilliQ) water at a constant applied force of around 1 nN and at a constant scanning rate of 0.2 lines per second.

All reported measurements were obtained using the same AFM probe consisting of a rectangular cantilever with a nominal spring constant of 0.18 N/m and a sharp pyramidal tip (20 nm nominal radius of curvature) with a wear-resistant coating to maintain the same tip geometry among the different scans, by using HQ:CS17/Hard/Al BS model (MikroMasch, Tallinn, Harju County, Estonia).

Roughness values were calculated from flattened topography images using the JPK Data Processing software. Root-mean-square roughness (R_q) values for the samples were calculated from seven AFM topography images taken on randomly selected. Median values, 25%–75% boxes, and out layers are represented.

2.2.5 | Fourier Transform Infrared Spectroscopy

FTIR-ATR spectra have been performed using a Nexus Thermonicolet instrument (Thermo Fisher Scientific, Waltham, Middlesex County, Massachusetts, USA) equipped with ATR accessory (diamond window), 100 scans, $4\,cm^{-1}$ resolution, DTGS detector, background air. Spectra were collected for all the samples in the range $4000–400\,cm^{-1}$ (mid-IR region). Each analysis has been repeated in different specimens and/or different points of the same sample.

2.2.6 | X-Ray Diffraction

Crystallographic properties of the polymeric samples were evaluated by X-ray diffraction at room temperature in air. PANalytical AERIS equipment (Malvern Panalytical, Almelo, Overijssel, Netherlands) was operated at 30 kV and 10 mA, with Bragg–Brentano geometry, Cu K_α radiation, angular range (2θ) of 15°–55°, 0.011° step size, Ni filter and PIXcel^{1D} detector. The total crystallinity percentage of the dense samples was estimated by using polymer crystallinity rate subroutine from Fullprof suite software [23]. The background was selected manually between 15° and 35°.

3 | Results

3.1 | Mechanical Tests

Pristine PLA is unsuitable for applications above its glass transition temperature ($T_g\approx60°C$) because it undergoes rapid softening and hydrolytic degradation, processes that are further accelerated under strongly alkaline conditions. Its mechanical performance is highly dependent on processing parameters, such as annealing treatments or the incorporation of additives. For example, a previously evaluated PLA grade (3251D) exhibited a Young's modulus of 2.5 GPa, an ultimate tensile strength (UTS) of 30 MPa, and an elongation at break of 2% [4].

Table 2 summarizes the mechanical properties (E_t, σ_M, ε_M, ε_B) of the C and RP benchmark samples before and after treatment at 70°C in an aqueous solution at pH 12. As expected, both C and RP composites exhibited higher stiffness than pristine PLA due to inorganic reinforcement, resulting in increased Young's modulus values compared with those reported for certain neat PLA grades [4].

Figure 1 presents the stress–strain curves of the C and RP benchmark samples before and after treatment at 70°C in an aqueous solution at pH 12. Both untreated C and RP benchmarks exhibit the characteristic behavior of rigid polymers, with a negligible plastic deformation region. The stress–strain curves show an initial linear elastic regime (whose slope corresponds to Young's modulus), followed by a slight decrease in slope without a well-defined transition to plastic flow, ultimately leading to brittle fracture. This brittle failure behavior is consistent with the stress–strain response of rigid polymers such as polystyrene or poly(methyl methacrylate) (PMMA), in which strain hardening is absent and fracture occurs shortly after yielding [24].

After treatment at 70°C in a strongly alkaline medium, all samples exhibited pronounced embrittlement, thus a lower toughness, as can be observed by an evident reduction of the area under the stress strain curve. The ultimate tensile strength decreased by approximately a factor of three in the C samples and

TABLE 2 | Young's modulus (E_t), UTS (σ_M) strain at UTS (ε_M), and strain at break(ε_B), together with standard deviations, of C and RP benchmark samples and after treatment at 70°C in aqueous solution at pH 12.

Sample	E_t (GPa)	σ_m (MPa)	ε_M (%)	ε_b (%)
RP benchmark	5.9 (0.1)	54.1 (0.4)	2.3 (0.1)	2.6 (0.5)
RP-70-12	6.0 (0.8)	23.8 (1.1)	0.4 (0.1)	0.4 (0.1)
C benchmark	6.0 (0.1)	79.7 (5.5)	2.1 (0.1)	2.1 (0.1)
C-70-12	5.1 (0.3)	24.7 (7.8)	0.7 (0.4)	0.7 (0.4)

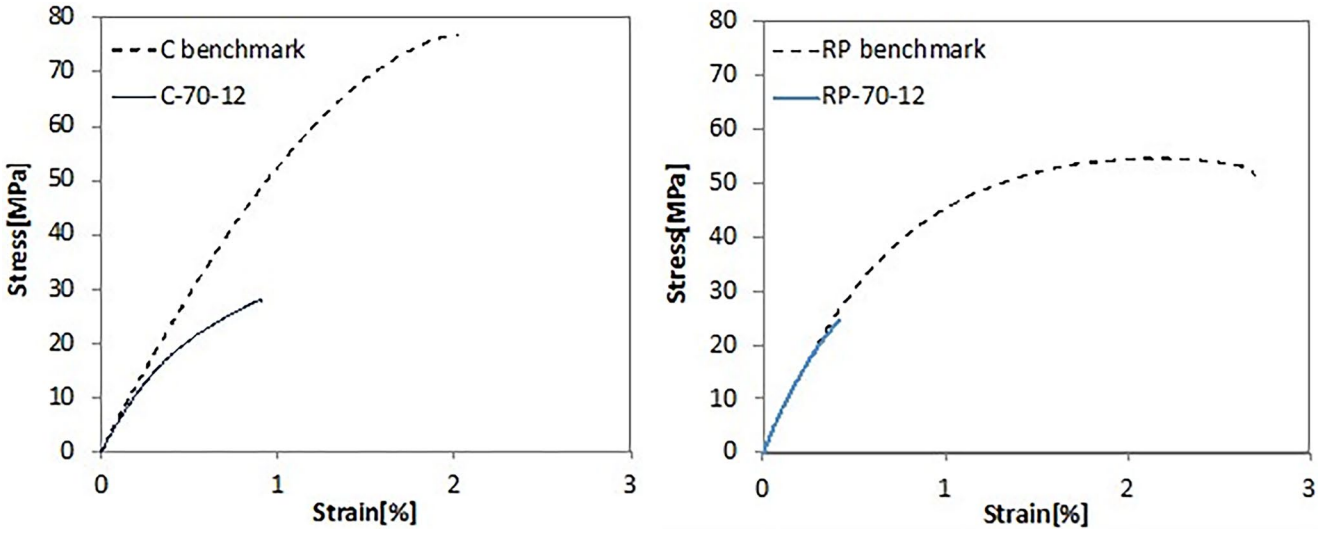

FIGURE 1 | Stress versus strain diagrams of tensile test on RP benchmark and RP samples treated at 70°C in pH = 12.

by about 50% in the RP samples, while the strain at break fell below 1%. These results indicate different extents of degradation among the materials. Temperature plays a critical role in this behavior, as exposure at 70°C, above the glass transition temperature of PLA ($T_g \approx 60$°C), enhances chain mobility and accelerates hydrolytic reactions, leading to substantially faster degradation compared with that occurring at room temperature [25]. The type of filler also influences the degradation process. The RP samples, which contain calcium silicate, exhibited greater resistance to harsh conditions than the C samples. Due to the shape factor, calcium silicate present as microparticles in the polymeric matrix reduces water permeability and slows hydrolytic degradation by limiting water diffusion into the polymer matrix [26]. In contrast, the C samples, which contain glass fibers-shape, exhibited limited hydrophobicity [27] and water penetrates these interfaces via capillary action, promoting rapid hydrolytic degradation under high-temperature and alkaline pH conditions. This accelerated hydrolysis stems from their susceptibility to corrosion and enhanced water uptake, driven by ion-exchange processes and dissolution mechanisms [28].

In sum, the slightly better retention of mechanical properties in the RP samples suggests that calcium silicates locally hindered water penetration; however, the increased chain mobility above the glass transition temperature (70°C) ultimately facilitated hydrolysis in both systems. These mechanical results therefore provide direct evidence that alkaline hydrolysis is the dominant degradation mechanism.

3.2 | Morphological Analysis

Figure 2 presents SEM micrographs of the RP and C benchmark samples, along with images of specimens treated at 70°C in an aqueous solution at pH 12. The benchmark samples exhibited relatively uniform surfaces with only minor roughness, composed of irregular particles approximately 50 μm in size and coated by a homogeneous layer that appeared continuous at higher magnification. After alkaline exposure, both composites showed clear signs of degradation, with filler-dependent features. In the C samples [4], the erosion of the polymer matrix led to the exposure of glass fibers. In contrast, the RP samples developed microcracks that propagated across the surface, indicating filler dissolution and localized stress concentrations (highlighted by yellow circles in Figure 2). These observations confirm that the type of reinforcement modulates the hydrolytic degradation pathways [25]. In this case, the glass fibers promote fiber–matrix decoupling and matrix erosion, whereas calcium silicate facilitates microcrack formation and partial dissolution.

3.3 | Wetting Analysis

Wettability is an intrinsic material property determined by intermolecular interactions, describing the extent to which a liquid droplet spreads over a solid surface. It is typically quantified by the static contact angle, which reflects the equilibrium

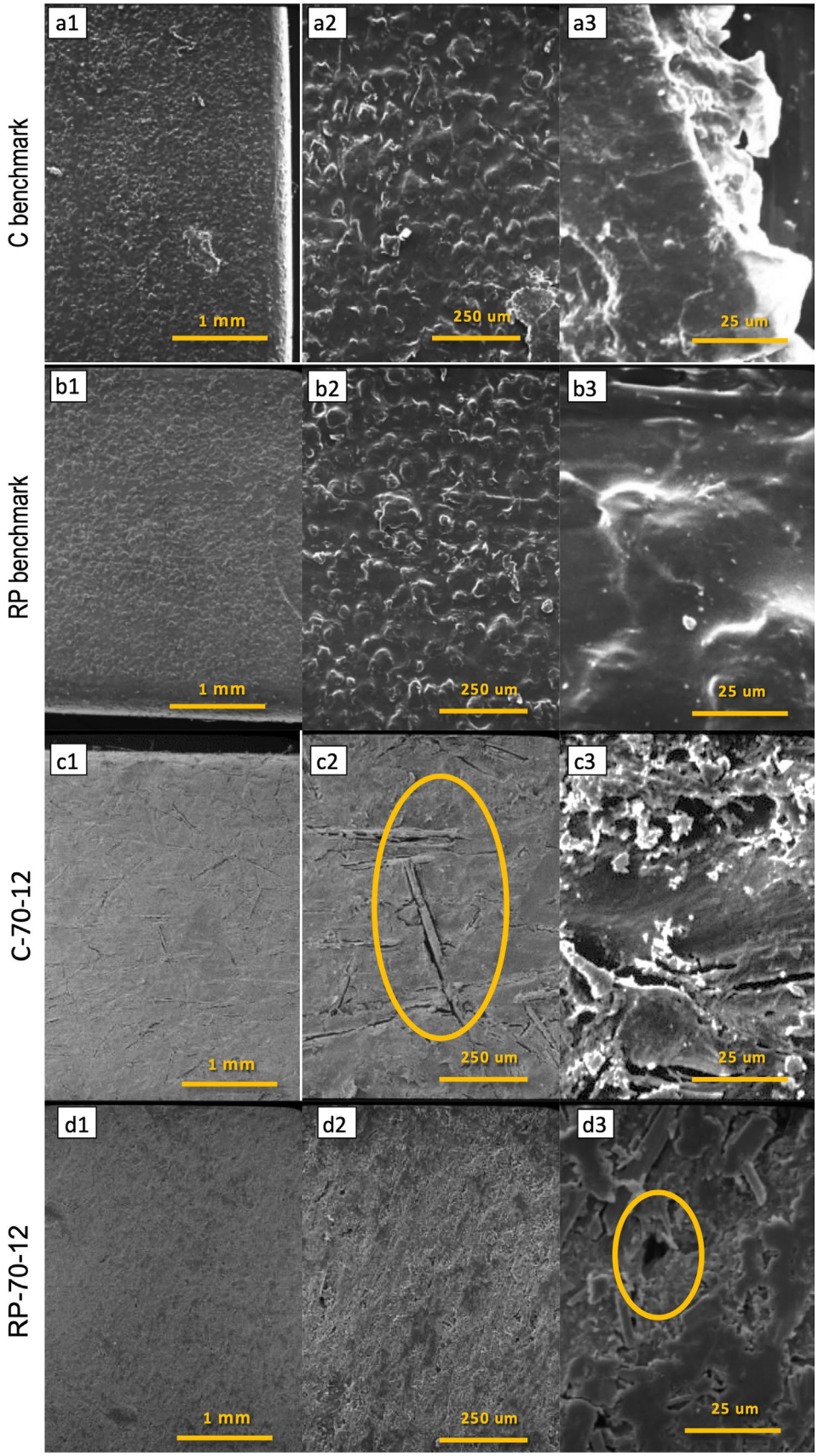

FIGURE 2 | SEM images at 25× (column 1, a1, b1, c1 and d1), 100× (column 2, a2, b2, c2 and d2), and 1000× (column 3, a3, b3, c3 and d3) of RP and C samples (benchmark and immersed at 70°C and pH = 12).

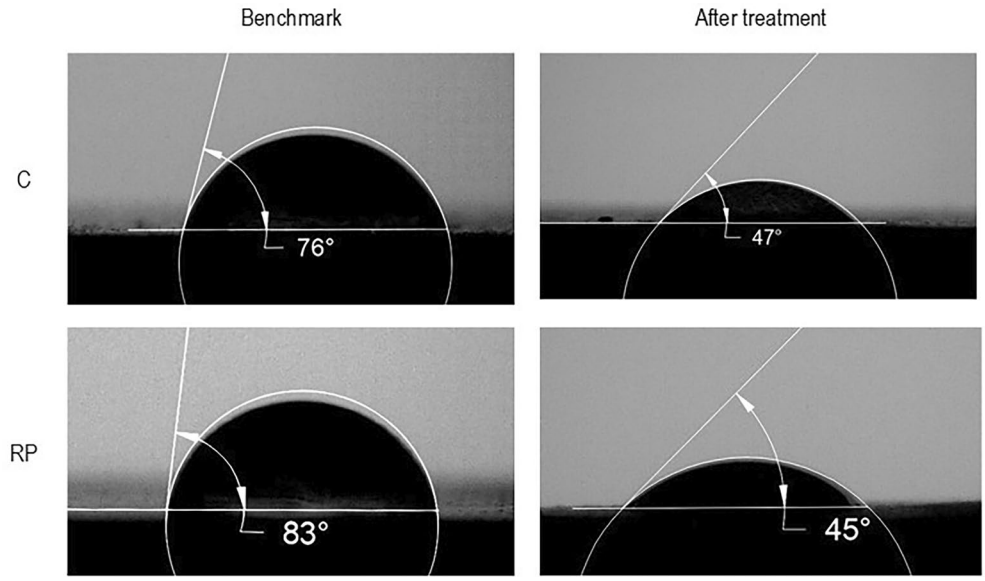

FIGURE 3 | Contact angle for a specimen of C and RP samples (respectively top and down), benchmark (left column) and after immersion at 70°C and pH = 12 (right column).

among the interfacial tensions of the solid, liquid, and vapor phases [29]. Wettability is influenced by both surface roughness and the chemical composition of the solid, and it correlates directly with hydrophobicity or hydrophilicity, thereby affecting hydrolytic degradation mechanisms [30, 31].

Figure 3 presents the wettability results for the C and RP samples before and after exposure to harsh conditions. Initially, the C benchmark samples exhibited higher wettability (74°±4°) than the RP benchmarks (82°±2°), suggesting a relatively great susceptibility to degradation. Contact angle measurements decreased substantially for both composites after treatment (C: $74° \pm 4° \rightarrow 48° \pm 0.5°$; RP: $82° \pm 2° \rightarrow 48° \pm 3°$), reaching the same level of wettability for both the samples, indicating an increased surface hydrophilicity. The increased wettability (i.e., decreased contact angles) can be related to the changing in the surface morphology that facilitates further water intake, reinforcing the positive feedback between chain scission and hydrolytic attack, as previously observed in the mechanical analysis (Section 3.1) and SEM imaging (Section 3.2). However, although the surfaces appeared geometrically flat, the presence of non-uniformly distributed micro-asperities partially affected measurement reproducibility. The errors values remain contained in the range of few angle degrees, suggesting that this evolution of the contact angle might be ascribed to a functional change in the nature of the surface. The enhanced hydrophilicity after treatment can be attributed to the formation of hydroxyl and carboxylate groups during alkaline hydrolysis, as will be discussed in Section 3.5, providing direct chemical evidence of surface modification.

3.4 | Roughness Analysis

Atomic force microscopy (AFM) provides a high-resolution view of surface topography. Results reported in this paragraph complement SEM observations of larger-scale morphology and enable quantitative assessment of surface degradation. AFM topography images were acquired from multiple randomly selected regions. Figure 4 presents representative topography images of the two samples before and after treatment. Analysis of the surface topography allows the calculation of changes in roughness parameters, which quantify treatment-induced structural modifications [32], including the root mean square roughness (R_q) values reported in Figure 5.

AFM revealed contrasting surface evolutions for the two sample types. In the C samples, surface roughness decreased, consistent with polymer layer erosion and surface smoothing following glass fiber dissolution, in agreement with previous studies on the degradation of PLA-based materials [33–35], which suggests that hydrophilic interfaces (e.g., glass fibers in the composites) accelerate degradation by promoting water infiltration and localized stress concentration [36]. The observed reduction in surface roughness is consistent with SEM characterizations of the treated C samples, which revealed the exposure of fibers following the dissolution of the external polymer layers, resulting in a smoother underlying surface (Section 3.2). Moreover, although wettability increased after alkaline treatment, this effect was less pronounced in the C samples compared with the RP samples (Section 3.3). In contrast, the RP samples exhibited increased roughness, with fractured domains reflecting silicate dissolution, which led to a disrupted surface and stress-induced cracking after treatment.

These differences underscore the filler-dependent roles in modulating surface morphology: erosion-driven smoothing in the C samples versus filler-assisted roughening in the RP samples. Both behaviors are consistent with a hydrolysis-driven degradation pathway, as inferred from SEM and FTIR analyses.

3.5 | FTIR-ATR Analysis

The spectra of RP and C benchmark materials are reported in Figures 6 and 7, and the assignation of the main IR bands is

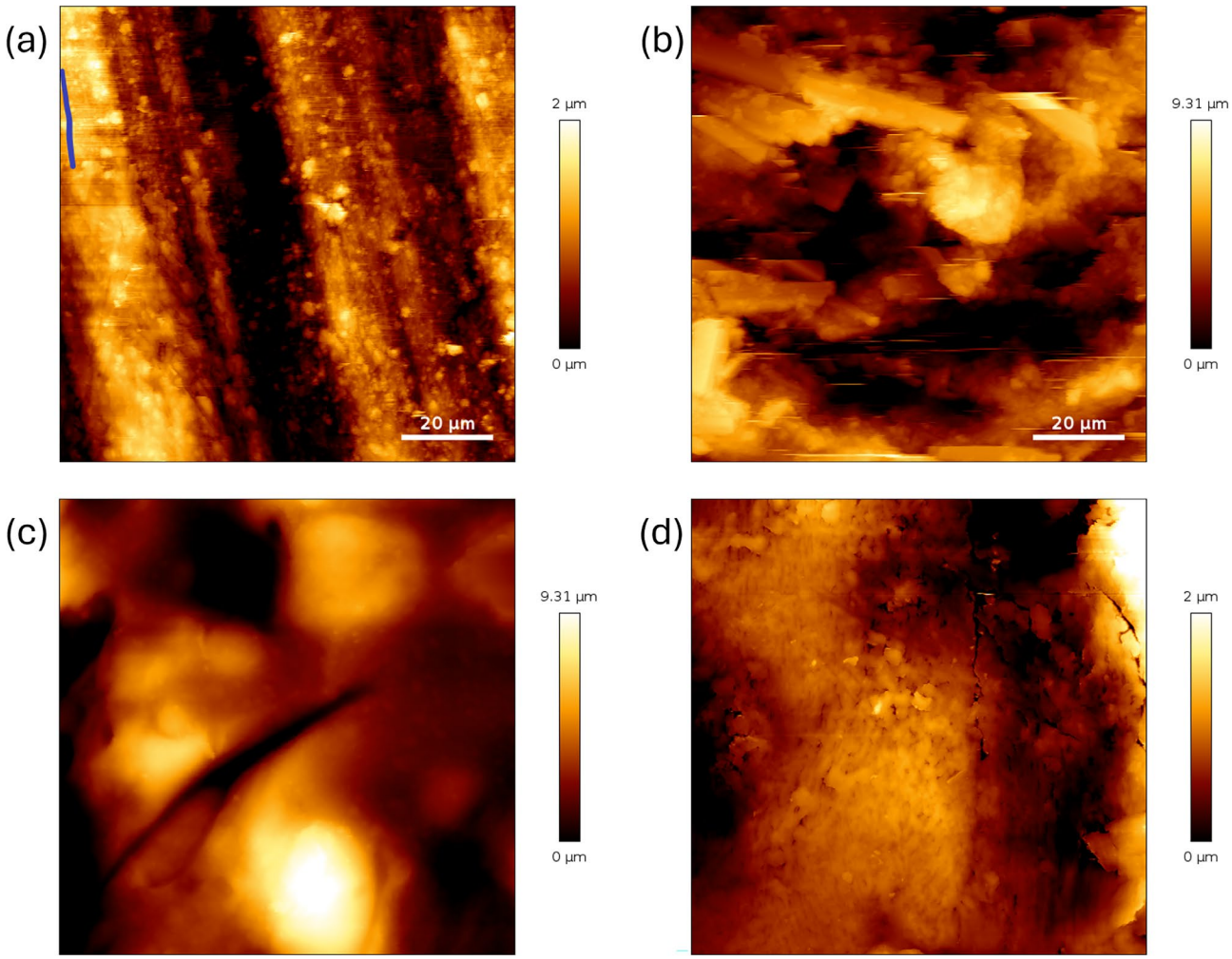

FIGURE 4 | Representative topography images of $100 \times 100\,\mu m^2$ regions of the RP (a, b) and C (c, d) samples. Images (a) and (c) refer to the samples before treatment while images (b) and (d) represent the samples after treatment.

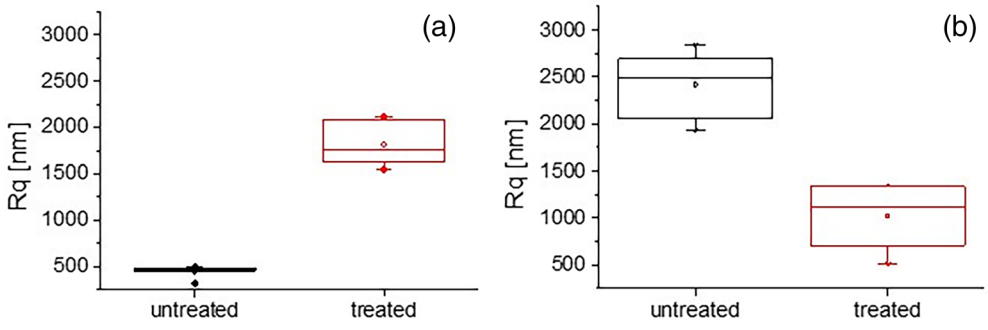

FIGURE 5 | Root-mean-square roughness (R_q) values for RP (a) and C (b) samples, calculated from seven AFM topography images taken on randomly selected $100 \times 100\,\mu m^2$ regions, before (untreated) and after treatment (treated). Median values, 25%–75% boxes, and outliers are represented.

highlighted in the same figures. A common feature in both spectra is a main complex band split with two maxima, centered at 1715–1720 cm^{-1} and 1755 cm^{-1}, and assigned to vC═O of ester groups. Namely, the component at 1755 cm^{-1} is characteristic of the PLA structure while the components at lower frequencies: near 1715, 1720, and 1735 cm^{-1} (deconvolution spectra in Figures S1 and S2), can be assigned to other ester compounds as well as to polymer chains in a different conformation and crystallization degree, and/or additives and secondary phases as also discussed in Section 3.6. The envelope of bands with maxima at 1212, 1180, 1157, 1130, 1085, 1045 cm^{-1} arises from C—O—C and C—C stretching modes, with contributions from CH_3 deformation modes. Weaker bands in the 1450–1330 cm^{-1} region are also assigned to CH deformation modes, whose corresponding stretching modes are detected in the range 3000–2850 cm^{-1} [37–41].

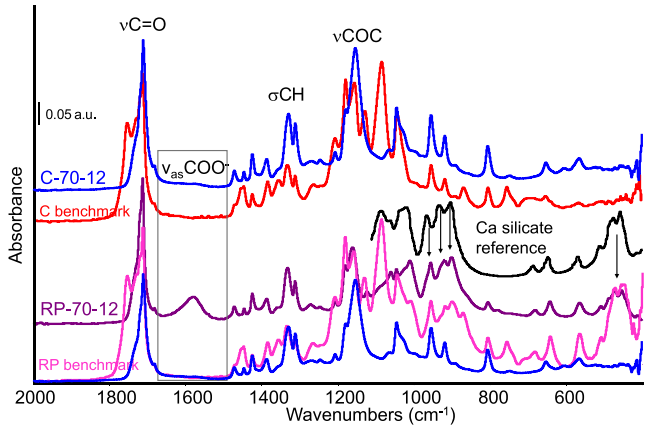

FIGURE 6 | FTIR-ATR spectra of samples RP and C (benchmark and after treatment at 70°C and pH = 12). Arrows: bands due to Ca-silicate filler.

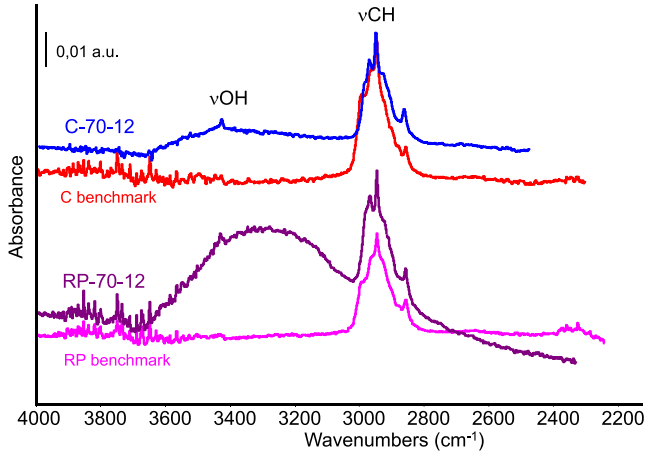

FIGURE 7 | ATR IR spectra of samples RP and C (benchmark and after treatment at 70°C and pH = 12). High frequency region.

In RP sample spectra, additional broad absorptions below 1000 cm^{-1} (namely bands at 965, 935, 900 cm^{-1} and 530–450 cm^{-1}) are observed (evidenced in Figure 6), attributed to vibrational modes of the inorganic silicate component of the material and overlapping with bands of the polymer matrix. Features specifically due to bioglass filler at 1100 and 800 cm^{-1} [42] are likely masked by strong polymer absorptions and cannot be detected in spectra of sample C.

Spectra of the samples after treatment at pH 12 and 70°C show several remarkable differences compared to the spectra of the pristine material (Figure 6 and deconvolution spectra in Figures S1 and S2). A common feature in both samples' spectra is the loss of one or more components in the 1750–1735 cm^{-1} range, the carbonyl stretching region, indicating the breaking of ester bonds [4]. The signals centered near 1715 cm^{-1} together with shoulders near 1730 and 1720 cm^{-1} are not affected by the high temperature treatment. In parallel, in the 1200–1000 cm^{-1} spectral range, the strong band at 1085 cm^{-1} disappears giving further evidence of alteration in the ester bonds. CH deformation modes in the spectral region also exhibit small shifts in shape and position.

A new band at 1580 cm^{-1} clearly appears in the spectrum of the RP sample after treatment, assigned to the asymmetric stretching mode of a carboxylate group —COO^-, whose corresponding symmetric stretching mode would be masked by the IR bands of polymer matrix near 1400 cm^{-1}. These features may relate to basic hydrolysis of ester groups, leading to the formation of carboxylate groups as the polymer chains are cleaved, and therefore explaining the accelerated degradation under our experimental conditions (i.e., alkaline environment and high temperature). The hydrolysis process would not be solely due to the prolonged heating in alkaline aqueous solution; it would be also enhanced by a catalytic effect of silica-based groups reported previously by Blaker et al. and Larranaga et al. [42, 43] for thermal degradation of PLA composites. Such degradation pathway could be catalyzed by the presence of silica-based filler due to the reaction occurring at the interface between a PDLLA matrix and bioglass particles. The high basicity will favor the formation of SiO^- active centers which behave as catalyst of the hydrolytic degradation.

In the low frequency region of the spectrum, the IR bands assigned to silicate species become more evident in the RP sample spectra after treatment. Likely, the microcracks detected by SEM analysis (Section 3.2) led to an increased exposition of the inorganic filler at the surface of the composite.

In the IR spectrum of sample C after treatment, a weak IR absorption appears as a shoulder near 1590 cm^{-1} (Figure S3) suggesting a similar behavior, that is basic hydrolysis leading to the formation of carboxylate groups, although at a limited extent. We must note that C composite exhibits a lower content of filler, in the form of fibers, thus exposing a low surface to the interaction with the polymer matrix. This is a further indication that the extent of degradation depends not only on the environment (pH, temperature) but also on the amount and on the properties of the filler, including its interaction with the matrix and its dispersion in the polymer matrix.

The high-frequency region of the post-treatment sample spectra (Figure 7) is characterized by a broad absorption centered at ~3450 cm^{-1} tailing toward lower frequencies, typical of H-bonded OH groups arising from an increased amount of adsorbed water molecules and/or newly exposed hydroxyl groups. The intensity of the hydroxyl peak is higher in the RP sample spectrum, in agreement with an increased hydrolysis of ester groups, as discussed in the previous paragraphs.

In sum, FTIR results confirm some ester bond cleavage through basic hydrolysis, directly linked to the carboxylate groups formation and the presence of exposed hydroxyl groups, in agreement with prior studies [44–46]. RP sample surface was most affected by the high-temperature, basic pH treatment as its hydrophilicity increased (in accordance with Section 3.4), due to enhanced exposure of hydroxyl groups.

3.6 | Crystallographic Analysis

PLA can exist as either an amorphous or semicrystalline polymer, depending on its chemical composition and thermal history [47]. Its physical, mechanical, and chemical properties are indeed strongly related to the crystalline structure

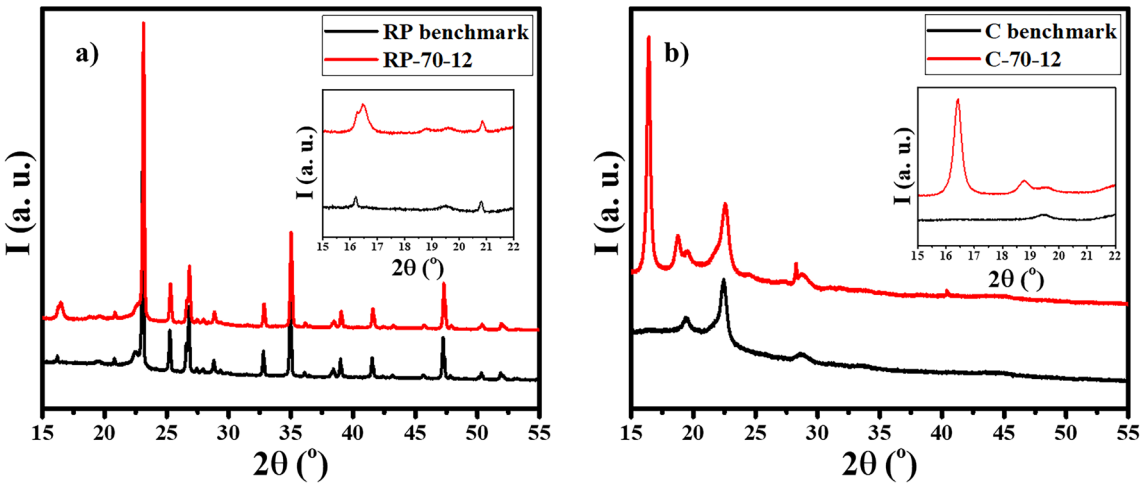

FIGURE 8 | Comparison between PLA samples before and after harsh conditions. XRD patterns of (a) RP and (b) C samples. The intensity (I) is expressed in arbitrary units (a. u.).

TABLE 3 | Estimated range of crystalline content of the dense samples, expressed in %.

	Benchmark		After harsh conditions	
	RP	C	RP	C
Crystallinity (%)	22–24	6–7	32–33	17–18

and degree of crystallinity. Moreover, hydrolytic degradation is also significantly influenced by the degree of crystallinity [48]. Figure 8 compares the changes in crystallinity for both polymers before and after exposure to high temperature and basic pH.

As reported in prior studies [49], pristine PLA primarily exists in an amorphous state and crystallizes in the α-form, characterized by XRD peaks near 14.8°, 16.8°, 19.0°, and 23°. Additional peaks may originate from the added fillers, industrial additives, secondary phases, or manufacturing artifacts, consistent with results from FT IR characterization (see the complexity of the C═O stretching mode signals). The XRD pattern of the RP benchmark also shows a low-intensity peak at 16.2°, tentatively attributed to the less common PLA δ-form under specific conditions [50]. After exposure to harsh conditions, peak intensities increase, reflecting a higher degree of crystallinity, as reported in Table 3. Overlapping peaks at 16.2° and 16.4°, together with the emergence of a new peak at 18.8°, suggest a shift toward α-form dominance. The persistent peak at 23° corresponds to the calcium silicate filler [51], which remains almost unaffected by the treatment, confirming that alterations of the PLA polymer chains represent the relevant degradation pathway as suggested by the IR results.

The XRD pattern of the C benchmark indicates an amorphous phase, as no characteristic peaks for PLA α- or δ-forms are observed between 16° and 19°. After exposure to harsh conditions, crystallization of the α-form is evident, with distinct peaks at 16.4° and 18.8°. Similarly, the prominent peaks at 19.4° and 22.5° are likely attributable to glass fibers.

Previous studies have shown that high crystallinity in PLA composites promotes selective degradation in amorphous regions, resulting in slit-like valleys and increased surface roughness [52], consistent with our observations in RP samples. Conversely, low crystallinity leads to more uniform degradation, reducing surface roughness through homogeneous erosion [52], in agreement with our findings in C samples. The inorganic filler, besides catalyzing the breaking of ester bonds, may act as a nucleating agent, contributing to the crystallization process.

Interestingly, RP-70-12 exhibits a systematic shift of XRD peaks toward higher angles compared to the RP benchmark, indicating reduced interplanar distances. This shift likely results from hydrogen bond formation or mild hydrolysis (via nucleophilic substitution) involving hydroxide ions (OH^-), polymer chains, and the inorganic filler in the basic environment. This hypothesis is supported by wetting analysis (Section 3.2), where the contact angle decreased from 83° to 45° after degradation due to increased H-bonded surface groups, and by FTIR data (Section 3.5), which show the emergence of a broad and strong band related to new hydroxy groups. This behavior is less pronounced in C samples, which also exhibited a smaller decrease in contact angle. The apparent increase in crystallinity, however, did not translate into improved mechanical performance. Instead, it reflects local reorganization of shorter chains produced by chain scission, which possess enhanced mobility and crystallize more readily. The net effect is embrittlement, demonstrating that the observed crystallinity increase serves as a marker of chain rearrangement rather than material strengthening.

4 | Discussion

The combined analysis of mechanical, morphological, spectroscopic, and crystallographic data provides a consistent picture of the degradation phenomena affecting PLA-based composites under harsh alkaline conditions. Filler type strongly modulates the degradation behavior. In both cases, the presence of SiO^- groups in the inorganic filler can act as a catalyst for the hydrolysis of ester bonds to carboxylate species [42, 43]. In the

C samples, a dissolution of the outer polymeric layer produced smoother surfaces (AFM) and exposed fiber (SEM), thereby accelerating hydrolytic attack. The faster degradation of biodegradable glass fibers compared to conventional glass fibers may also contribute to facilitating the decomposition of the polymer matrix, as the progressive loss of fiber integrity can increase porosity and accessibility to water and microorganisms [53], promoting the biodegradation of the polymer phase. In contrast, the RP samples containing calcium silicate exhibited increased surface roughness and microcrack formation, consistent with partial filler dissolution and enhanced water uptake. Calcium silicate may also act as a nucleating agent, promoting crystallization of the remaining polymer, which explains the more pronounced increase in crystallinity compared with the C samples.

Despite the observed increase in crystallinity (XRD), both composites experienced significant losses in tensile strength and ductility. This apparent contradiction can be rationalized by considering that chain scission initially occurs in the amorphous domains, generating shorter chains with enhanced mobility that reorganize into more ordered, crystalline structures. The disappearance of at least one component in the C═O stretching region of the IR spectra may support this hypothesis. However, the extensive reduction in molecular weight weakens the overall material, resulting in embrittlement and failure at low strain. Thus, the increase in crystallinity reflects local reorganization of surviving chains rather than a global improvement in mechanical integrity.

Hydroxide ions promote cleavage of ester bonds, leading to chain scission and the formation of hydroxyl and carboxylate end groups, as evidenced by the broad OH band (~3450 cm^{-1}) and the COO^- band (1580–1590 cm^{-1}). These findings confirm that alkaline hydrolysis is the primary degradation pathway.

Overall, the results highlight the complex interplay between filler chemistry, chain scission, and morphological reorganization in determining the long-term durability of these composites. Although the number of samples was limited, consistent trends across independent measurements (mechanical testing, SEM, AFM, FTIR, and XRD) reinforce the validity of the conclusions. Nevertheless, further studies with larger sample sets and molecular weight characterization (e.g., GPC) are required to quantify chain scission and confirm the proposed degradation mechanism.

5 | Conclusions

This study demonstrates that commercial PLA biocomposites for multi-use cutlery (glass fiber-reinforced) and rigid packaging (calcium silicate-reinforced) undergo distinct degradation pathways when exposed to harsh alkaline, dishwasher-like conditions (70°C, pH 12, 30 days), confirming their vulnerability during repeated industrial cleaning cycles.

Mechanical testing revealed severe embrittlement in both composites, with ultimate tensile strength dropping ~70% for cutlery (80 → 25 MPa) and ~55% for packaging (54 → 24 MPa), and strain at break falling below 1% primarily due to hydrolytic chain scission above T_g that reduces matrix ductility. Surface analyses (SEM/AFM) showed reinforcement-specific damage: glass fiber dissolution caused matrix erosion and fiber exposure in cutlery samples, while calcium silicate triggered microcracking and dramatic roughness increases in packaging samples. FTIR-ATR confirmed ester hydrolysis (reduced C═O, increased OH/COOH), while XRD revealed higher crystallinity post-aging, indicating chain reorganization as amorphous regions degrade preferentially.

These findings highlight the complex interplay between environmental factors, reinforcement type, and polymeric matrix in determining the long-term durability of PLA-based composites and fill a critical gap by systematically comparing their performance under realistic dishwasher conditions. Calcium silicate composites showed better mechanical retention despite more severe surface damage, suggesting localized filler hydration slows bulk water diffusion, whereas glass fibers accelerate matrix loss through corrosion. Future research should focus on optimizing the composition and processing of bioplastics to enhance their resistance to harsh conditions, thereby promoting their wider adoption in demanding applications.

Author Contributions

Cristina Moliner: conceptualization, investigation, writing – original draft, writing – review and editing. **Alberto Lagazzo:** conceptualization, investigation, writing – original draft, writing – review and editing. **Juan Felipe Basbus:** investigation, writing – original draft, writing – review and editing. **Roberto Raiteri:** investigation, writing – original draft. **Elisabetta Finocchio:** conceptualization, investigation, writing – original draft, writing – review and editing, validation. **Elisabetta Arato:** conceptualization, funding acquisition, project administration.

Acknowledgments

This work was supported by the European Union's Horizon 2020—Research and Innovation Framework Programme through the research project BIO-PLASTICS EUROPE (Grant agreement No. 860407). Open access publishing facilitated by Universita degli Studi di Genova, as part of the Wiley - CRUI-CARE agreement.

Funding

This work was supported by the European Union's Horizon 2020—Research and Innovation Framework Programme through the research project BIO-PLASTICS EUROPE (Grant agreement No. 860407).

Conflicts of Interest

The authors declare no conflicts of interest.

Data Availability Statement

The data that support the findings of this study are available from the corresponding author upon reasonable request.

References

1. A. K. Behera, S. S. Pattnaik, C. Mohanty, R. Srivastav, and J. Pradhan, "Mechanical and Cytotoxic Analysis of Cutlery Developed From Phenol-Formaldehyde Modified Soy-Jute Composite," *Vietnam Journal of Chemistry* 62, no. 2 (2024): 151–159, https://doi.org/10.1002/vjch.202200162.

2. M. E. González-López, S. de Jesus Calva-Estrada, M. S. Gradilla-Hernández, and P. Barajas-Álvarez, "Current Trends in Biopolymers

for Food Packaging: A Review," *Frontiers in Sustainable Food Systems* 7 (2023): 1–20, https://doi.org/10.3389/fsufs.2023.1225371.

3. K. C. Bishoyi, S. S. Pattnaik, D. Behera, and A. K. Behera, "Effect of Banana Peduncle Fiber on the Mechanical, Water, and Degradation Properties of Hybrid Composites Made From Modified Soy Resin," *Polymer Composites* 44, no. 10 (2023): 6604–6615, https://doi.org/10.1002/pc.27583.

4. E. Finocchio, C. Moliner, A. Lagazzo, S. Caputo, and E. Arato, "Water Absorption Behavior and Physico-Chemical and Mechanical Performance of PLA–Based Biopolymers Filled With Degradable Glass Fibers," *Journal of Applied Polymer Science* 140, no. 43 (2023): 1–13, https://doi.org/10.1002/app.54578.

5. H. Ramezani Dana and F. Ebrahimi, "Synthesis, Properties, and Applications of Polylactic Acid-Based Polymers," *Polymer Engineering and Science* 63, no. 1 (2023): 22–43, https://doi.org/10.1002/pen.26193.

6. Y. Wu, X. Gao, J. Wu, T. Zhou, T. T. Nguyen, and Y. Wang, "Biodegradable Polylactic Acid and Its Composites: Characteristics, Processing, and Sustainable Applications in Sports," *Polymers* 15, no. 14 (2023): 3096, https://doi.org/10.3390/polym15143096.

7. V. Nagarajan, A. K. Mohanty, and M. Misra, "Perspective on Polylactic Acid (PLA) Based Sustainable Materials for Durable Applications: Focus on Toughness and Heat Resistance," *ACS Sustainable Chemistry & Engineering* 4, no. 6 (2016): 2899–2916, https://doi.org/10.1021/acssuschemeng.6b00321.

8. S. S. Ray and M. Okamoto, "Biodegradable Polylactide and Its Nanocomposites: Opening a New Dimension for Plastics and Composites," *Macromolecular Rapid Communications* 24, no. 14 (2003): 815–840, https://doi.org/10.1002/marc.200300008.

9. S. Saravana and R. Kandaswamy, "Investigation on the Mechanical and Thermal Properties of PLA/Calcium Silicate Biocomposites for Injection Molding Applications," *Silicon* 11, no. 2 (2019): 1143–1150, https://doi.org/10.1007/s12633-018-9926-9.

10. N. Tripathi, M. Misra, and A. K. Mohanty, "Durable Polylactic Acid (PLA)-Based Sustainable Engineered Blends and Biocomposites: Recent Developments, Challenges, and Opportunities," *ACS Engineering au* 1, no. 1 (2021): 7–38, https://doi.org/10.1021/acsengineeringau.1c00011.

11. M. Ghasemlou, C. J. Barrow, and B. Adhikari, "The Future of Bioplastics in Food Packaging: An Industrial Perspective," *Food Packaging and Shelf Life* 43 (2024): 101279, https://doi.org/10.1016/j.fpsl.2024.101279.

12. Bioleader, 2026, https://www.bioleaderpack.com/biodegradable-cutlery-compostable-utensils-white-paper-2025/.

13. A. Lagazzo, C. Moliner, E. Finocchio, S. Caputo, and E. Arato, "Hydrolytic Degradation and Assessment of Performance of PLA and PBS-Based Plastics Designed for Packaging Applications," *International Journal of Polymeric Science* 2025, no. 1 (2025): 1–16, https://doi.org/10.1155/ijps/5602847.

14. E. A. Growney Kalaf, K. R. Hixon, P. U. Kadakia, A. J. Dunn, and S. A. Sell, "Electrospun Biomaterials for Dermal Regeneration," in *Electrospun Materials for Tissue Engineering and Biomedical Applications* (Elsevier, 2017), 179–231, https://doi.org/10.1016/B978-0-08-101022-8.00005-3.

15. D. Cam, S. Hyon, and Y. Ikada, "Degradation of High Molecular Weight Poly(l-Lactide) in Alkaline Medium," *Biomaterials* 16, no. 11 (1995): 833–843, https://doi.org/10.1016/0142-9612(95)94144-A.

16. H. Tsuji, "Hydrolytic Degradation," in *Poly(Lactic Acid)* (Wiley, 2022), 467–516, https://doi.org/10.1002/9781119767480.ch21.

17. S. J. de Jong, E. R. Arias, D. T. S. Rijkers, C. F. van Nostrum, J. J. Kettenes-van den Bosch, and W. E. Hennink, "New Insights Into the Hydrolytic Degradation of Poly(Lactic Acid): Participation of the Alcohol Terminus," *Polymer (Guildf)* 42, no. 7 (2001): 2795–2802, https://doi.org/10.1016/S0032-3861(00)00646-7.

18. F. Codari, S. Lazzari, M. Soos, G. Storti, M. Morbidelli, and D. Moscatelli, "Kinetics of the Hydrolytic Degradation of Poly(Lactic Acid)," *Polymer Degradation and Stability* 97, no. 11 (2012): 2460–2466, https://doi.org/10.1016/j.polymdegradstab.2012.06.026.

19. M. Karamanlioglu, R. Preziosi, and G. D. Robson, "Abiotic and Biotic Environmental Degradation of the Bioplastic Polymer Poly(Lactic Acid): A Review," *Polymer Degradation and Stability* 137 (2017): 122–130, https://doi.org/10.1016/j.polymdegradstab.2017.01.009.

20. E. Blázquez-Blázquez, R. Barranco-García, T. M. Díez-Rodríguez, M. L. Cerrada, and E. Pérez, "Role of the Plasticizers on the Crystallization of PLA and Its Composites With Mesoporous MCM-41," *Journal of Materials Science* 59, no. 15 (2024): 6305–6321, https://doi.org/10.1007/s10853-024-09556-x.

21. P. Gao and D. Masato, "The Effects of Nucleating Agents and Processing on the Crystallization and Mechanical Properties of Polylactic Acid: A Review," *Micromachines (Basel)* 15, no. 6 (2024): 776, https://doi.org/10.3390/mi15060776.

22. J. Muller, A. Jiménez, C. González-Martínez, and A. Chiralt, "Influence of Plasticizers on Thermal Properties and Crystallization Behaviour of Poly(Lactic Acid) Films Obtained by Compression Moulding," *Polymer International* 65, no. 8 (2016): 970–978, https://doi.org/10.1002/pi.5142.

23. J. Rodríguez-Carvajal, "Recent Advances in Magnetic Structure Determination by Neutron Powder Diffraction," *Physica B: Condensed Matter* 192, no. 1–2 (1993): 55–69, https://doi.org/10.1016/0921-4526(93)90108-I.

24. I. M. Ward, *Mechanical Properties of Solid Polymers*, 2nd ed. (Wiley, 1983).

25. S. Farah, D. G. Anderson, and R. Langer, "Physical and Mechanical Properties of PLA, and Their Functions in Widespread Applications—A Comprehensive Review," *Advanced Drug Delivery Reviews* 107 (2016): 367–392, https://doi.org/10.1016/j.addr.2016.06.012.

26. B. Haasnpour and V. M. Karbhari, "Characteristics and Models of Moisture Uptake in Fiber Reinforced Composites: A Topical Review," *Polymers* 16, no. 16 (2024): 2265, https://doi.org/10.3390/polym16162265.

27. L. Calabrese, D. Badagliacco, C. Sanfilippo, and V. Fiore, "Flax–Glass Fiber Reinforced Hybrid Composites Exposed to a Salt-Fog/Dry Cycle: A Simplified Approach to Predict Their Performance Recovery," *Polymers* 15, no. 11 (2023): 2542, https://doi.org/10.3390/polym15112542.

28. A. E. Krauklis and A. T. Echtermeyer, "Long-Term Dissolution of Glass Fibers in Water Described by Dissolving Cylinder Zero-Order Kinetic Model: Mass Loss and Radius Reduction," *Open Chemistry* 16, no. 1 (2018): 1189–1199, https://doi.org/10.1515/chem-2018-0133.

29. P. M. M. Pereira, A. S. Moita, G. A. Monteiro, and D. M. F. Prazeres, "Characterization of the Topography and Wettability of English Weed Leaves and Biomimetic Replicas," *Journal of Bionic Engineering* 11, no. 3 (2014): 346–359, https://doi.org/10.1016/S1672-6529(14)60048-2.

30. S. Vasi, G. Ceccio, A. Cannavò, P. Pleskunov, and J. Vacík, "Study of Wettability of Polyethylene Membranes for Food Packaging," *Sustainability* 14, no. 10 (2022): 5863, https://doi.org/10.3390/su14105863.

31. N. Slepickova Kasalkova, P. Slepicka, Z. Kolska, and V. Svorcik, "Wettability and Other Surface Properties of Modified Polymers," in *Wetting and Wettability* (InTech, 2015), https://doi.org/10.5772/60824.

32. R. Liu, S. Zhang, C. Zhao, et al., "Regulated Surface Morphology of Polyaniline/Polylactic Acid Composite Nanofibers via Various Inorganic Acids Doping for Enhancing Biocompatibility in Tissue Engineering," *Nanoscale Research Letters* 16, no. 1 (2021): 4, https://doi.org/10.1186/s11671-020-03457-z.

33. S. Schusser, S. Menzel, M. Bäcker, et al., "Degradation of Thin Poly(-Lactic Acid) Films: Characterization by Capacitance–Voltage, Atomic Force Microscopy, Scanning Electron Microscopy and Contact-Angle Measurements," *Electrochimica Acta* 113 (2013): 779–784, https://doi.org/10.1016/j.electacta.2013.08.025.

34. A. Melelli, D. Pantaloni, E. Balnois, et al., "Investigations by AFM of Ageing Mechanisms in PLA-Flax Fibre Composites During Garden Composting," *Polymers (Basel)* 13, no. 14 (2021): 2225, https://doi.org/10.3390/polym13142225.

35. D. Palma-Ramírez, A. M. Torres-Huerta, M. A. Domínguez-Crespo, D. Del Angel-López, A. I. Flores-Vela, and D. de la Fuente, "Data Supporting the Morphological/Topographical Properties and the Degradability on PET/PLA and PET/Chitosan Blends," *Data in Brief* 25 (2019): 104012, https://doi.org/10.1016/j.dib.2019.104012.

36. P. Fryń, S. Lalik, K. A. Bogdanowicz, N. Górska, A. Iwan, and M. Marzec, "Degradation of Hybrid Material PLA: 5CB: SWCN Under the Influence of Neutral, Acidic, and Alkaline Environments," *RSC Advances* 13, no. 6 (2023): 3792–3806, https://doi.org/10.1039/D2RA05350K.

37. N. Choksi and H. Desai, Synthesis of Biodegradable Polylactic Acid Polymer by Using Lactic Acid Monomer, 2017, http://www.ripublication.com.

38. G. Kister, G. Cassanas, and M. Vert, "Effects of Morphology, Conformation and Configuration on the IR and Raman Spectra of Various Poly(Lactic Acid)s," *Polymer (Guildf)* 39, no. 2 (1998): 267–273, https://doi.org/10.1016/S0032-3861(97)00229-2.

39. C. Moliner, E. Finocchio, E. Arato, G. Ramis, and A. Lagazzo, "Influence of the Degradation Medium on Water Uptake, Morphology, and Chemical Structure of Poly(Lactic Acid)-Sisal Bio-Composites," *Materials* 13, no. 18 (2020): 3974, https://doi.org/10.3390/ma13183974.

40. A. A. Cuadri and J. E. Martín-Alfonso, "Thermal, Thermo-Oxidative and Thermomechanical Degradation of PLA: A Comparative Study Based on Rheological, Chemical and Thermal Properties," *Polymer Degradation and Stability* 150 (2018): 37–45, https://doi.org/10.1016/j.polymdegradstab.2018.02.011.

41. J. R. Rocca-Smith, A. Lagorce-Tachon, C. Iaconelli, et al., "How High Pressure CO2 Impacts PLA Film Properties," *Express Polymer Letters* 11, no. 4 (2017): 320–333, https://doi.org/10.3144/expresspolymlett.2017.31.

42. J. J. Blaker, A. Bismarck, A. R. Boccaccini, A. M. Young, and S. N. Nazhat, "Premature Degradation of Poly(α-Hydroxyesters) During Thermal Processing of Bioglass-Containing Composites," *Acta Biomaterialia* 6, no. 3 (2010): 756–762, https://doi.org/10.1016/j.actbio.2009.08.020.

43. A. Larrañaga and J.-R. Sarasua, "Effect of Bioactive Glass Particles on the Thermal Degradation Behaviour of Medical Polyesters," *Polymer Degradation and Stability* 98, no. 3 (2013): 751–758, https://doi.org/10.1016/j.polymdegradstab.2012.12.015.

44. H. Y. Tan, E. Widjaja, F. Boey, and S. C. J. Loo, "Spectroscopy Techniques for Analyzing the Hydrolysis of PLGA and PLLA," *Journal of Biomedical Materials Research. Part B, Applied Biomaterials* 91B, no. 1 (2009): 433–440, https://doi.org/10.1002/jbm.b.31419.

45. R. Vaid, E. Yildirim, M. A. Pasquinelli, and M. W. King, "Hydrolytic Degradation of Polylactic Acid Fibers as a Function of pH and Exposure Time," *Molecules* 26, no. 24 (2021): 7554, https://doi.org/10.3390/molecules26247554.

46. C. Lors, P. Leleux, and C. H. Park, "State of the Art on Biodegradability of Bio-Based Plastics Containing Polylactic Acid," *Frontiers in Materials* 11 (2025): 1–14, https://doi.org/10.3389/fmats.2024.1476484.

47. A. J. Müller, M. Ávila, G. Saenz, and J. Salazar, "CHAPTER 3. Crystallization of PLA-Based Materials," in *Poly(Lactic Acid) Science and Technology: Processing, Properties, Additives and Applications*, ed. A. Jiménez, M. Peltzer, and R. Ruseckaite (Royal Society of Chemistry, 2014), 66–98, https://doi.org/10.1039/9781782624806-00066.

48. G. Kortaberria, C. Marieta, A. Jimeno, P. Arruti, and I. Mondragon, "Crystallization of Poly(–Lactid Acid) Monitored by Dielectric Relaxation Spectroscopy and Atomic Force Microscopy," *Journal of Microscopy* 224, no. 3 (2006): 277–289, https://doi.org/10.1111/j.1365-2818.2006.01701.x.

49. G. Wang, D. Zhang, B. Li, G. Wan, G. Zhao, and A. Zhang, "Strong and Thermal-Resistance Glass Fiber-Reinforced Polylactic Acid (PLA) Composites Enabled by Heat Treatment," *International Journal of Biological Macromolecules* 129 (2019): 448–459, https://doi.org/10.1016/j.ijbiomac.2019.02.020.

50. L. Zhang, G. Zhao, and G. Wang, "Investigation on the α/δ Crystal Transition of Poly(l-Lactic Acid) With Different Molecular Weights," *Polymers* 13 (2021): 3280.

51. I. A. W. B. Siqueira, S. S. Amaral, N. K. de Moura, et al., "In Vitro Bioactivity and Biological Assays of Porous Membranes of the Poly(Lactic Acid) Containing Calcium Silicate Fibers," *Polymer Bulletin* 77, no. 10 (2020): 5357–5371, https://doi.org/10.1007/s00289-019-03021-5.

52. J. Shi, J. Zhang, Y. Zhang, et al., "Crystallinity Dependence of PLLA Hydrophilic Modification During Alkali Hydrolysis," *Polymers* 15, no. 1 (2022): 75, https://doi.org/10.3390/polym15010075.

53. I. Lyyra, K. Leino, T. Hukka, M. Hannula, M. Kellomäki, and J. Massera, "Impact of Glass Composition on Hydrolytic Degradation of Polylactide/Bioactive Glass Composites," *Materials (Basel)* 14, no. 3 (2021): 667, https://doi.org/10.3390/ma14030667.

Supporting Information

Additional supporting information can be found online in the Supporting Information section. **Figure S1:** Deconvolution of the IR spectra of sample RP benchmark (a) and after treatment at 70°C and pH = 12 (b). **Figure S2:** Deconvolution of the IR spectra of sample C benchmark (a) and after treatment at 70°C and pH = 12 (b). **Figure S3:** Magnification of the IR spectra of samples C and RP after treatment at 70°C and pH = 12. COO^- stretching region.